Probing Atmospheric Aerosol by Multi-modal Mass Spectrometry Techniques: Revealing Aging Characteristics of its Individual Molecular Components

Kyla S.A. Siemens,¹ Demetrios Pagonis,^{3,4,†} Hongyu Guo,^{3,4} Melinda K. Schueneman,^{3,4} Jack E Dibb,⁵ Pedro Campuzano-Jost,^{3,4} Jose- L. Jimenez,^{3,4} Alexander Laskin^{1,2}*

Present Address: Department of Chemistry & Biochemistry, Weber State University, Ogden, Utah 84403, USA

KEYWORDS. Biomass Burning, Organic Aerosol, FIREX-AQ, Mass Spectrometry, Liquid Chromatography, Atmospheric Aging, Chemical Characterization, Sulfur-containing Organics.

ABSTRACT: Detailed chemical characterization of biomass burning organic aerosol (OA) was performed using a synergistic combination of multi-modal mass spectrometry techniques. OA was analyzed in-situ using a high-resolution time-of-flight aerosol mass spectrometer (HR-ToF-AMS) and an extractive electrospray ionization time-of-flight mass spectrometer (EESI-MS) deployed onboard the NASA DC-8 research aircraft. Additionally, complementary filter samples of OA were collected for offline laboratory analysis using high performance liquid chromatography interfaced with a photodiode array and an electrospray ionization high resolution mass spectrometer (HPLC-PDA-HRMS). During a research flight on August 3rd, 2019, which was focused on the Williams Flats Fire, WA, the onboard HR-ToF-AMS data revealed the abundant presence of organic-sulfur (OS) species as prominent components of the OA. These OS species were identified based on their unique fragmentation. Further investigation using HPLC-PDA-HRMS and MSⁿ fragmentation allowed us to identify the molecular characteristics of these unusual OS species. The dominant OS compounds detected during the research flight were found to be alkyl benzene sulfonates. Organosulfate, nitroaromatic, and oxygenated aromatic components of OA were also identified. Guided by the HRMS results, time-resolved aging profiles of selected individual OA species were retrieved from the real-time EESI-MS datasets to evaluate their aging evolution in the emission plume. Notably, the alkyl benzene sulfonate species showed remarkable stability over 8 hours of atmospheric transport. In contrast, common organosulfates displayed short apparent half-life times, that were as low as 1.2 hours, indicating their susceptibility to aging. The nitroaromatic and oxygenated aromatic species exhibited relatively slower aging, with average apparent half-life times of 1.8 and 2.2 hours, respectively.

¹Department of Chemistry, Purdue University, West Lafayette, Indiana 47907, USA

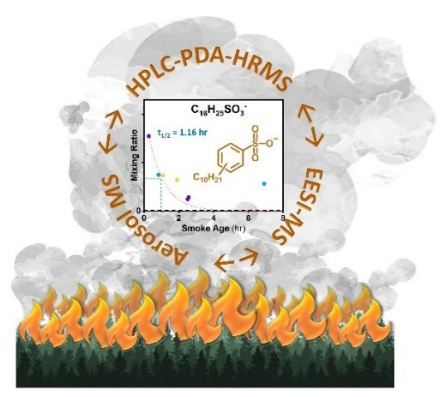
²Department of Earth Atmospheric and Planetary Sciences, Purdue University, West Lafayette, Indiana 47907, USA

³Department of Chemistry, University of Colorado, Boulder, Colorado 80309, USA

⁴Cooperative Institute for Research in Environmental Sciences, University of Colorado, Boulder, Colorado, 80309, USA

⁵Earth System Research Center, University of New Hampshire, Durham, New Hampshire 03824, USA

^{*}Corresponding Author: alaskin@purdue.edu



INTRODUCTION.

Atmospheric organic aerosols (OA) contain components of primary emissions from biogenic and anthropogenic sources (POA) and products of atmospheric reactions that convert volatile organic species into secondary organic aerosol (SOA).^{1–3} As they age in the atmosphere, POA and SOA undergo transformations driven by various atmospheric processes such as oxidation, photolysis, fragmentation, oligomerization, gas-to-particle partitioning, and cloud processing, which blur their original identity.⁴

Wild and prescribed forest fires, burning of biomass for heating and cooking, and practices of burning waste and crop residues emit very complex mixtures of biomass burning organic aerosol (BBOA) with significant atmospheric concentrations. 5 BBOA has a profound influence on Earth's radiative forcing, air quality, and human health. Specifically, direct effects on radiative forcing include absorption and scattering of sunlight and terrestrial radiation by airborne particles.^{2,6} The indirect effects are related to aerosol-induced changes in the cloud albedo and cloud lifetime. 7-10 The majority of OA scatters incoming solar radiation and thus has a cooling effect on climate; however its light-absorbing components, termed brown carbon (BrC), 11 absorb light in the near-UV range, 12 and therefore contribute to a warming effect.^{13,14} Additionally, BBOA, and more generally OA, degrade air quality, which causes serious human health implications ranging from allergy, respiratory, and cardiovascular diseases to reduced life-expectancy. 15 Because adverse effects of OA on humans and the environment depend strongly on its chemical composition, it is essential to characterize OA with sufficient molecular specificity.

The sensitivity and specificity of field-deployable in-situ mass spectrometry techniques for aerosol characterization is continually evolving, offering valuable insights into the chemical composition of OA. 16-19 However, these techniques have certain limitations, such as their inability to separate isomers and lower mass resolution and sensitivity compared to laboratory instrumentation. The complexity of the real-world OA is too great to be unraveled by online techniques alone. Offline analysis of field-collected OA samples by high performance liquid chromatography interfaced with a photodiode array detector and an electrospray ionization high-resolution mass spectrometer (hereafter HPLC-PDA-HRMS) is a comprehensive method capable of characterizing species of interest and providing their elemental and molecular descriptions based on the separation and accurate measurements of ion masses and their MSn fragmentation patterns. 20-28 Obtained molecular information complements the limited specificity of in-situ mass spectrometry techniques.

In this work, we present the synergistic implementation of multi-modal mass spectrometry techniques. Specifically, in-situ measurements were performed using an Aerodyne high-resolution time-of-flight aerosol mass spectrometer (HR-ToF-AMS, or AMS hereafter), 19 and an extractive electrospray ionization time-of-flight mass spectrometer (EESI-ToF-MS, hereafter EESI-MS), complemented by offline HPLC-PDA-HRMS measurements of the collected sample. This combined approach allows us to explore the chemical evolution of individual molecular components of BBOA in greater depth than is possible with any single technique alone. In this case study, OA from wildfires was analyzed in-situ using an AMS and an EESI-MS deployed onboard the NASA DC-8 research aircraft. In parallel, bulk samples of OA were collected for subsequent offline laboratory analysis using a HPLC-PDA-HRMS. The in-situ collected AMS data is used to identify specific OA-type classes. The information retrieved from the AMS measurements then guides the HPLC-PDA-HRMS data acquisition and data mining of specific components of interest, which in turn informs processing and interpretation of the individual molecular species observed by the EESI-MS and allows derivation of specific molecular aging profiles.

EXPERIMENTAL.

Real-time MS measurements. Fire Influence on Regional to Global Environments and Air Quality (FIREX-AQ)²⁹ was the field study where we initially implemented this novel multimodal MS approach for OA characterization. Chemical composition of airborne aerosols was monitored in real-time by the AMS and EESI-MS instruments (Aerodyne Research, Inc. Billerica, MA, USA) deployed onboard the DC-8 research aircraft during the FIREX-AQ campaign conducted over northwestern and southeastern US in summer 2019.²⁹ This work focuses on the research flight on August 3rd, 2019 (21:00-03:45 UTC) which probed the emission plume from the Williams Flats fire in Washington state.

The AMS, a commonly used field instrument for *in-situ* quantitative measurements of common OA-type classes, ^{19,30} was one of the core aerosol characterization tools employed on the aircraft. ¹⁷ Recently developed EESI-MS is a novel technique capable of probing quantitative contributions of individual particulate organic molecules in real time. ^{18,31–33} Previously, an EESI-MS has been employed in several laboratory and ground field studies of OA constituents. ^{33–41} Combining the use of an AMS and an EESI-MS onboard the aircraft offers complementary advantages, with the broad class-specific OA description provided by the AMS guiding the investigation of time-resolved molecular components detected by the EESI-MS. Both instruments were operated continuously for the entirety of the flight. The

AMS provides *in-situ* quantitative field measurements of common OA-type classes at a mass resolution of $m/\Delta m = 3600$ at m/z 184, and the EESI-MS is used to probe time-resolved quantitative contributions of individual OA components at a mass resolution of $m/\Delta m = 3900$ at m/z 185 in positive polarity, and 3800 at m/z 154 in negative polarity. ^{18,31–33} EESI polarity was switched between flights, negative polarity was used for the Aug 3rd, 2019 flight discussed here. Data acquisition and interpretation of the EESI-MS and AMS data have been discussed in detail in our previous manuscripts. ^{16,18,42,43} ^{44,45}

Real Time Mist Chamber Ion Chromatography Measurements. A custom mist chamber—ion chromatograph (referred hereafter as SAGA-MC-IC) system to measure nitric acid and ionic particle species with diameters up to nominally 1 $\mu m^{17,45}$ was also deployed on the DC-8 during FIREX-AQ. The MC (or Cofer scrubber) has been extensively used to collect water-soluble gases or particles. 46-48 Ambient air is drawn into a glass chamber where a continuously generated mist at slightly above ambient temperature (50 °C) uptakes both aerosols and soluble gases. After a fixed sample collection period (for FIREX-AQ this was 150 s), liquid is removed from the glass chamber and immediately analyzed with an online ion chromatography system. The ICs are custom built using primarily Dionex parts. Anions were separated using an AS-11 column and NaOH eluent. Two MC chambers and two ICs are run in parallel to provide continuous coverage.

In the planetary boundary layer the particle size range probed by AMS is closely comparable to that of the particle size range probed by SAGA-MC-IC. However, at higher altitudes the particle size cut of SAGA-MC-IC shifts smaller.¹⁷ For the data discussed here (\sim 4 km altitude) no large biases are expected. Reported accuracy (1σ) is 15% for the sulfate measurement.

All hazards and risks associated with the research flight operation were evaluated and mitigated by the aircraft crew according to their standard procedures and policies. No unexpected or unusually high safety hazards were encountered during operation of our instruments onboard the aircraft.

Field Collected Samples. During the FIREX-AQ campaign BBOA samples were regularly collected on a Teflon filter (polytetrafluoroethylene (PTFE), 0.45 µm porosity, 47 mm diameter, Whatman) for subsequent offline analysis (Figure S1). OA mass loadings on the collected filters were calculated based on inlet flowrate, collection time, and OA concentration measured by the AMS instrument. The filter sample from the research flight was collected during the first full pass over the smoke plume between 22:00 and 00:00 UTC on August 3rd, 2019. The flight path employed semi-Lagrangian sampling of the smoke plume, as illustrated in Figure 1. The aircraft altitude is plotted as a function of time in Figure S2. The AMS measurements revealed elevated concentrations of unusual sulfur-containing organic species in the smoke plume. The Teflon filter had a mass loading of 125 µg of OA collected from the smoke plume. Approximately 31 µg of OA was extracted from ¼ filter into 5 mL of acetonitrile (OptimaTM LC/MS grade, Fisher Chemical) by sonication for 20 minutes. Insoluble impurities were filtered from the sample with a pre-wetted PTFE membrane syringe filter (0.45 µm, FisherbrandTM). Fresh solvent was then used to rinse the extraction vial and was also filtered with the PTFE membrane syringe filter to recover remaining analytes. Extracts were then partially evaporated to ~250 μL and subsequently reconstituted to ~620 µL with water (OptimaTM LC/MS grade,

Fisher Chemical), resulting in the final OA concentration of 50.5 mg/L for offline chemical analysis.

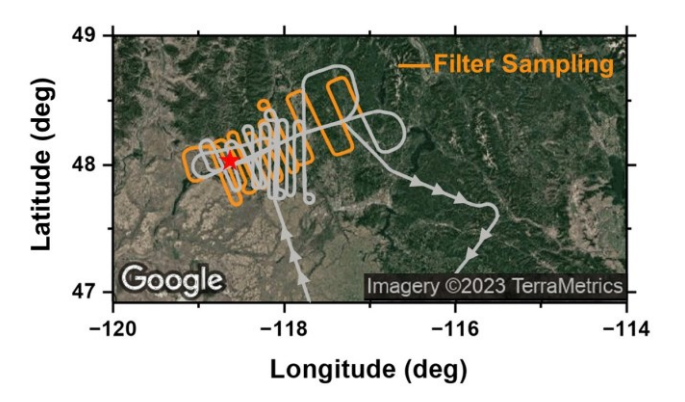


Figure 1. Semi-Lagrangian flight path of NASA DC-8 research aircraft during sampling of the Williams Flats fire, WA, on August $3^{\rm rd}$, 2019 (21:00-03:45 UTC). The portion of the flightpath highlighted in orange, corresponds to the first pass. Online measurements (AMS and EESI-MS) and filter sampling performed during the first pass is used for this work. Arrowheads on flight path indicate flight direction.

Offline Chemical Characterization. Laboratory analysis of the sample extract was performed using an analytical platform of HPLC (VanquishTM), coupled with a PDA detector and high resolution Orbitrap Q-Exactive HF-X mass spectrometer equipped with an electrospray ionization (ESI) source operated in negative mode (all components by Thermo Scientific Inc.) illustrated in Figure S1B. OA analyte components were separated on a reversed-phase column (Luna C18(2), L×I.D.: 150 × 2 mm, 5 µm particles, 100 Å pores, Phenomenex Inc.). The column compartment was maintained at a temperature of 25 °C. An injection volume of 25 μ L (1.26 μ g of OA) was introduced into the HPLC. A 110 min LC gradient adapted from Lin et al, 20 was employed. A binary mobile phase consisting of LC-grade water (A) and acetonitrile (B), both doped with 0.1% (v/v) formic acid (OptimaTM LC/MS grade, Fisher Chemical), at a flow rate of 0.2 mL/min, was used. The employed LC gradient was: 0-3 min at 10% B, 3-90 min linear ramp up to 100% B, 90-100 min hold at 100% B, 100-103 min linear ramp down to 10% B, 103-130 min hold at 10% B to re-equilibrate the column for the next run. The PDA detector employs a 10 mm LightPipe flow cell and a deuterium lamp. Continuous UV-Vis scans were collected at 200-680 nm wavelengths with a spectral resolution of 2 nm and acquisition frequency of 20 Hz. Eluting analytes were ionized using an ESI source operated in negative mode (-) at the following settings: capillary temperature of 250°C, 45 arbitrary units of sheath gas, 10 units of auxiliary gas, 2 units of sweep gas, and spray voltage of 3.5 kV. (-)ESI was used due to its sensitivity toward oxygenated aromatic compounds including OS species, nitroaromatics, and oxygenated aromatic hydrocarbons, all of which are of interest in this study. Mass spectra were recorded for the m/z range of 80-1200 Da at a mass resolution of $m/\Delta m = 240,000$ at m/z 200, and at RF level 80. The mass spectrometer was calibrated using standard CalMix solutions (Thermo Scientific, PI-88324).

Offline Tandem MS Experiments. Tandem MS experiments were conducted using an LTQ XL mass spectrometer equipped with an ESI source (all components by Thermo Scientific Inc.). The (–)ESI source was operated with the following settings: 10

arbitrary units of sheath gas, 5 units of auxiliary gas, 5 kV of spray voltage, 250° C capillary temperature, -32 V capillary voltage, and -110 V tube lens voltage. Collision energies ranging from 25-45 eV were optimized for MS² and MS³ experiments. Mass spectra were recorded for the m/z range of 50-2000 Da at a mass resolution of $m/\Delta m = 571$ at m/z 400. The mass spectrometer was calibrated using standard CalMix solutions (Thermo Scientific, PI-88324).

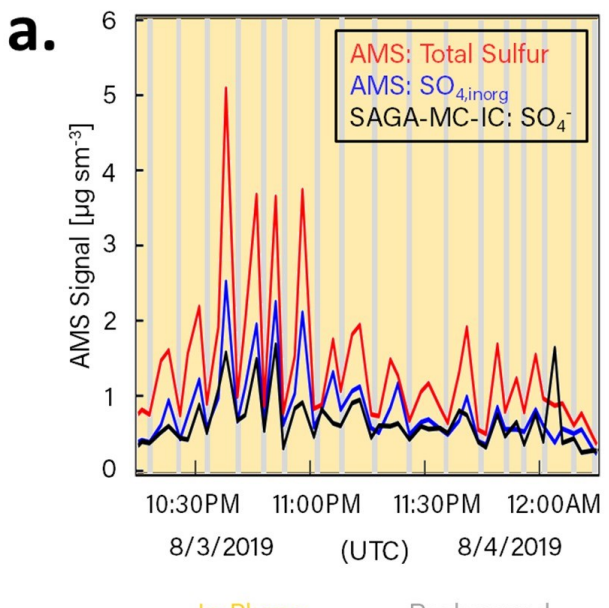
HRMS Data Analysis. Raw HPLC-PDA-HRMS data was initially viewed using Xcalibur software (Thermo Scientific Inc.). Subsequently, an open-source Mzmine (http://mzmine.github.io/)49,50 was used to perform peak picking, peak deconvolution, chromatogram construction, and peak smoothing. Raw Xcalibur data was imported into Mzmine, and low intensity peaks were filtered out using a threshold ion intensity of 3×10⁴ A.U. Chromatograms were constructed with a tolerance of 2.7 ppm. Custom built Excel macros⁵¹ and the MIDAS molecular formula calculator (v1.1; https://fs.magnet.fsu.edu/~midas/download.html) were used to assign formulas and eliminate erroneous assignments based on the first- and second-order Kendrick mass defects. The following limits were applied when assigning formulas: C_{c<50}H_{h<100}O₀₋₃₀N₀₋₃S₀₋₁ and a mass tolerance of \pm 2.7 ppm. 284 peaks were identified within the selected threshold, eluting over 0-100 min. Of the total peaks, 122 peaks (43%) were assigned with elemental formulas. 50, 24, and 48 peaks were CHOS, CHON, and CHO compounds.

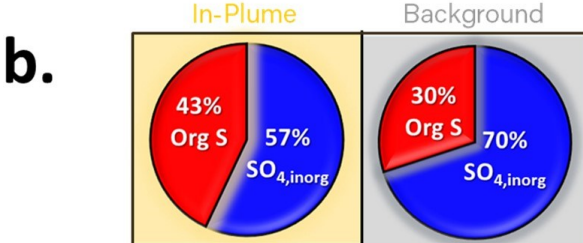
RESULTS AND DISCUSSION. The aircraft-based OA measurements of the wildfire emissions are challenging to quantify because measurements are continuous while passing in and out of a constantly diluting emission plume. To gain insights into the quantitative evolution of OA components in these complex emission plumes, onboard time-resolved measurements by the AMS and EESI-MS were employed (at 1 Hz measurement frequency for the flight discussed here). Measurements by these techniques are then compared and scaled with respect to the simultaneously measured carbon monoxide (CO) mixing ratio. 52-55 Because of the high emission rates, CO is used as an inert tracer to distinguish between the in-plume and the ambient air measurements and to account for the plume dilution with surrounding background air. 18,56-59

Figure 2a shows the time-resolved AMS records of total sulfur and inorganic sulfate, along with the complementary IC record of inorganic sulfate. Combined together, these records are used to distinguish between 'in-plume' and 'background' aerosol composition. Total sulfur signal by the AMS is deconvoluted into organic-sulfur (OS) and inorganic sulfate components with the methods assessed in Scheunemann et al¹⁶ and previously applied to the FIREX-AQ dataset in Rickly et al. 42 This included validation of the estimation by comparison to the inorganic sulfur factors derived by positive matrix factorization analysis (PMF) of the AMS data. 60 The values of sulfur apportionment are then compared with the IC measurement (recorded in 150 s averages) to further evaluate accuracy of the inorganic sulfate fraction determined by AMS. 61,62 Pie charts shown in Figure 2b illustrate fractions of OS and inorganic sulfate averaged over 'in-plume' and 'background' portions of the flight ('background' is defined as having less than 20% time coverage insmoke for the 150 s averaging interval of the SAGA-MC-IC instrument). The OS fraction measured by the AMS is substantially (~45%) greater 'in-plume', indicating emissions of OS

from wildfires and/or formation of OS through atmospheric aging reactions in the plume. Figure 2c shows a scatter plot of the AMS- and the IC- derived datasets, segregated again by inplume/background conditions. As expected, given the substantial amount of non-inorganic sulfate apportioned in the AMS, total AMS sulfate is larger than IC-sulfate; however, apportioned inorganic sulfate under background conditions agrees well within uncertainties for both instruments. This is not quite the case under in-plume conditions, but this is likely due to the less than ideal overlap between both instruments and the smoke plume at these low time resolutions.

Assessment of the AMS ion intensities indicates that the ion precursors are neither inorganic sulfates nor common organo-sulfates, ¹⁶ suggesting abundant presence of an as-yet unidentified subclass of OS species. ^{16,42,61} However, molecular information on the chemical forms of sulfur cannot be inferred from the AMS measurements alone. We employed a HPLC-PDA-HRMS platform to investigate the molecular composition of the unusual OS components of aerosol highlighted by the AMS.





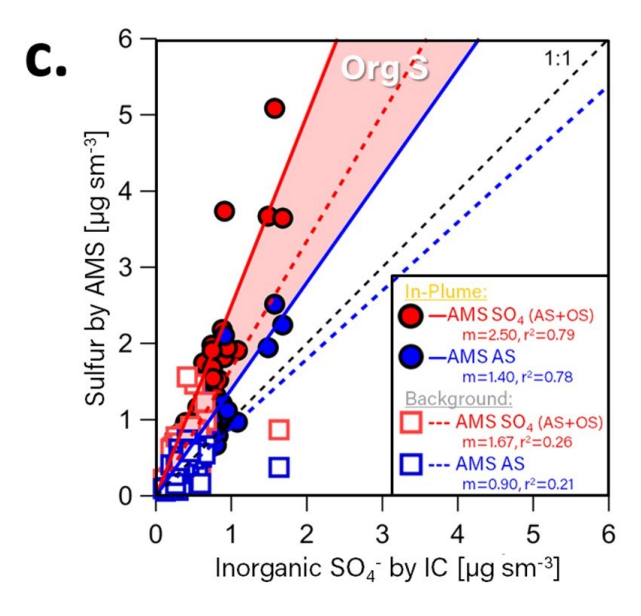


FIGURE 2. Airborne measurements of sulfur containing species in aerosol phase during August 3rd flight of the FIREX-AQ 2019 campaign. Panel (a) shows time-resolved measurements of the AMS total sulfur (red), inorganic sulfate (blue), and SAGA-MC-IC inorganic sulfate (black). Panel (b) shows pie charts indicating mass fractions of organic sulfur (red) and inorganic sulfate (blue) for the 'inplume' aerosol and the 'background' aerosol measured by the AMS. Panel (c) shows the correlation plot between mass concentration of total sulfur (red) and inorganic sulfate (blue) measured by the AMS both 'in-plume' (circles) and 'background' (squares), as a function of inorganic sulfate measured by SAGA-MC-IC. Linear orthogonal distance

regression fits are shown along with Pearson's correlation coefficients.

Figure 3 displays the (–)ESI-HRMS features detected over the entire LC separation run, providing an effective summary of the most abundant ions detected in the analyzed extract. Detailed information on the assigned species is included in the SI file, Table S1. Based on the formula assignments, we identify three main groups of species: CHOS – likely a mixture of commonly formed organo-sulfates⁴² and uncommon OS, CHO – mostly oxygenated aromatic hydrocarbons, and CHON – mostly nitroaromatics. Additionally, a few CHONS species were also observed. Figure 4 showcases the LC elution profiles of major species detected by HRMS, to aid in the identification and confirmation of individual species in each main group.

Within the observed CHOS species, several subgroups were distinguished, namely HSO₄-, RSO₃-, RSO₄-, RSO₅-, RSO₆-, and RSO₇. Of note, the maximum oxidation state associated with sulfur is (IV), therefore oxygen atoms in excess of O₄ have to be bound to the hydrocarbon (R) chain. The summed MS intensities of each CHOS subgroup are included in Figure S3. Their relative abundancies from most to least abundant are: HSO₄⁻> $RSO_3^- > RSO_4^- > RSO_5^- > RSO_7^- > RSO_6^-$. Deprotonated sulfuric acid (HSO₄-) is the most abundant ion in the entire sample, with m/z intensity >10⁹ A.U. This observation is expected in BBOA and is supported by the presence of the ³²S and ³⁴S isotopic peak pair at the expected m/z ratio (~20:1) within the unretained LC feature. Because of its strong affinity to the polar mobile-phase and weak attraction to the stationary phase, deprotonated sulfuric acid elutes in the first few minutes of the LC run as it is not retained on the column.

The next most intense CHOS subgroup, RSO₃, is an order of magnitude lower than the ion intensity of deprotonated sulfuric acid, with m/z intensity of RSO₃ around 10^8 A.U. (Figure S3). Correlated ³²S and ³⁴S isotopic peak pairs are unambiguously discernable for major RSO₃ species C₁₆H₂₅SO₃ and C₁₈H₂₉SO₃ , which have m/z intensities of approximately 10^7 A.U. and 10^8 A.U., respectively. In addition to the isotopic pairs, acetonitrile (+CH₃CN) and sodium formate (+NaHCO₂) adducts were also identified for the most abundant RSO₃ species. These adducts are listed in Table S1 and provide additional support to the unambiguous detection of RSO₃ species in the wildfire OA sample. Finally, the LC elution profiles presented in Figure 4, reveal that RSO₃ species elute between ~40-80 minutes. The highly abundant species C₁₆H₂₅SO₃ and C₁₈H₂₉SO₃ have multiple elution times, likely from structural isomers. Organosulfates, the most frequently reported type of OS in BBOA, contain RSO₄ groups. Both AMS (see detailed discussion in Rickly et al;⁴² this is further supported by the PMF factors retrieved for this flight) and HRMS measurements detect an abundant fraction of OS that is not attributed specifically to organosulfates, indicating the presence of another type of OS. The abundant fraction of species detected by HRMS that contains an -RSO3 group instead of the expected -RSO₄ group appears to make up the majority of these unusual OS species.

The RSO₄⁻ subgroup is the third most abundant group, with a summed MS intensity of approximately 10^7 A.U. Within this group, $C_{12}H_{25}SO_4$ ⁻ stands out as the most abundant ion with an m/z intensity around 2.5×10^6 A.U. $C_{12}H_{25}SO_4$ ⁻ is abundant enough to clearly observe the ³⁴S isotopic peak. As depicted in Figure 4, the major RSO₄⁻ species have slightly later LC elution times compared to RSO₃⁻ species. This trend is expected because the -SO₃ functional group is more polar than the -SO₄

group, and therefore has a higher affinity to the mobile phase. Like the RSO₃⁻ species, many RSO₄⁻ compounds also elute at multiple RTs, which indicates presence of their multiple isomers. Based on previous literature reports it is likely that the majority of these RSO₄⁻ species are common organosulfates originating from reactions of oxygenated organics with sulfuric acid produced by oxidation of sulfur dioxide (SO₂) emissions.⁴² The RSO_{>4}⁻ subgroups constitute a smaller overall fraction of the sample but follow similar trends to the RSO₄⁻ subgroup. These species likely also consist of organosulfates containing the -SO₄ functional group, with additional oxygens bound elsewhere on the carbon chain of molecules.

Moving on to the CHO and CHON products, their LC-MS elution profiles are displayed in Figure 4. Notably, the elution profiles of CHO species are characteristically narrower compared to those of CHOS species, likely due to fewer potential isomers for the smaller CHO species. Overall, CHO species elute over a wider range of retention times, with the smaller species (#C<8) appearing earlier because of their generally higher polarity or fewer active sites interacting with the stationary phase of the column. The LC elution profiles of the smaller CHON

species exhibit similar characteristics to the major CHO species; however, the larger CHON species have broader peaks and more isomers, akin to CHOS species.

Previous studies investigating the molecular composition of wildfire OA reported the abundant presence of oxidized aromatic hydrocarbons and nitroaromatics, 27,63-67 which were also detected in our analysis. As an example, Fleming et al. performed 12 unique biomass material burns to study composition and properties of biofuel-specific BrC chromophores.²⁷ The majority of these oxidized aromatic hydrocarbons and nitroaromatics are also reported here. Fleming et al. also reports specific species that were unique to single sources. Of these, we report C₁₀H₁₀O₂, which was detected only in subalpine fir burns. Notably, Douglas-fir-Pacific, Ponderosa Pine, and Oceanspray trees are the primary biofuels reported for the Williams Flats fire, WA.²⁹ Budisulistiorini et al. also report the presence of organosulfates in BBOA,63 consistent with our findings. Additionally, some of these studies utilized similar offline HRMS platforms for OA characterization,²⁷ which is the primary technique employed here to characterize newly reported species in this work, such as the RSO₃ subgroup.

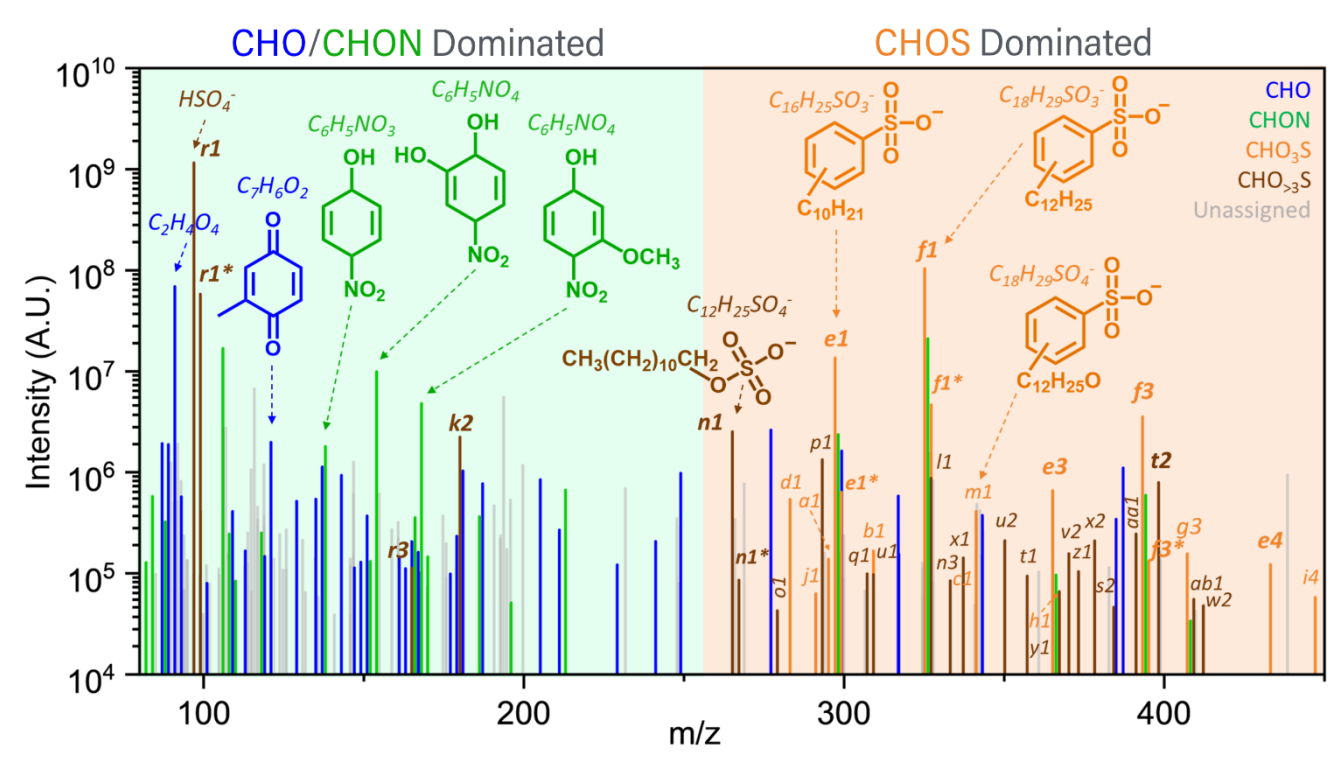


FIGURE 3. An (–)ESI-HRMS spectrum of the August 3^{rd} sample extract integrated across the LC run. Assigned peaks are color-coded as shown in the legend: CHO (blue), CHON (green), CHO₃S (orange), CHO_{>3}S (brown), and unassigned (grey). $C_{18}H_{29}SO_4$ is grouped with CHO₃S peaks because later MSⁿ analysis reveals that it is "alkyl benzene sulfonate-like" (ABS-like) in nature. OS species containing adducts are grouped according to the compound class of their corresponding parent ion. Annotations correspond to peaks listed in Table S1. '*' denotes a ^{34}S isotope. Peaks with intensities less than 3×10^4 A.U. are removed for clarity.

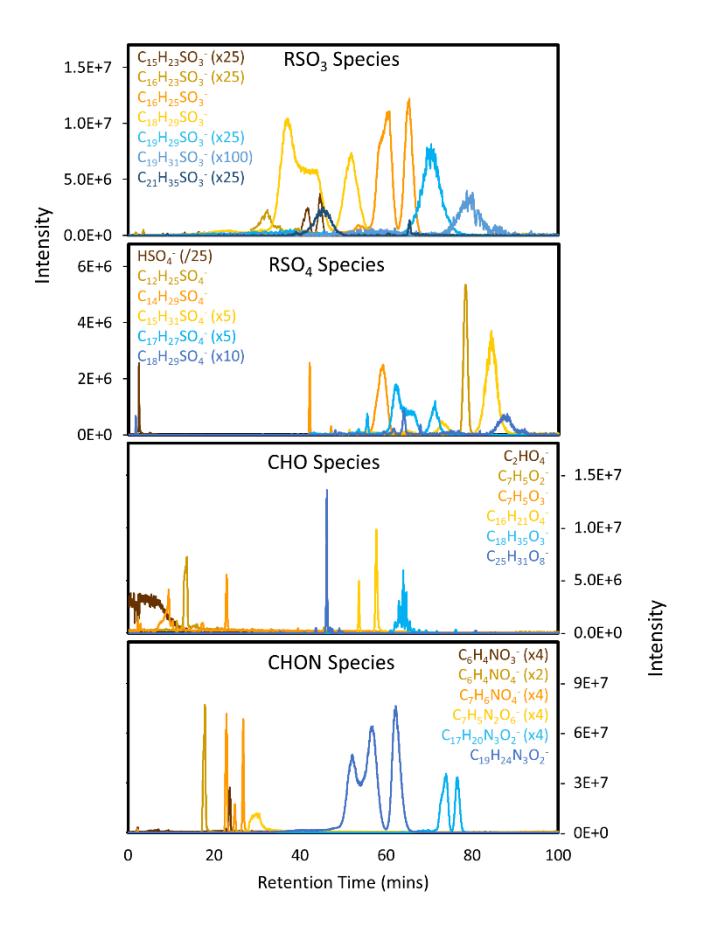


FIGURE 4. Extracted ion chromatograms of LC-separated components: RSO₃, RSO₄, CHO, and CHON selected species of interest. All species are color-coded as noted by the corresponding legends. Scaling factors of substantially higher and lower intensity species are indicated in brackets.

Analysis of the HPLC-PDA-HRMS data, including assessment of isotopic features, LC retention times, elution profiles, and comparison with literature are helpful for identification of OA species; however, tandem MSⁿ fragmentation experiments are needed for unequivocal identification and structural elucidation of individual OA species. Figure 5a illustrates MS² spectra of the parent ion C₁₈H₂₉SO₃ detected in the collected sample, compared to its commercially available isomer 4-Dodecylbenzene sulfonic acid (DBSA). In both cases, deprotonated C₁₈H₂₉SO₃⁻ parent ions (m/z 325) show very similar MS² fragmentation patterns. Their most prominent MS² fragments include m/z 170, 183, 197, and 261. All observed fragments and their relative intensities detected in the ambient sample resemble MS² fragments of DBSA. 68-72 Furthermore, additional MS3 fragmentation experiments with fragments m/z 183 and 261 also show remarkable consistency between the DBSA and the ambient sample. Specifically, Figure 5b shows the MS³ fragmentation pattern of $C_8H_7SO_3^-$ (m/z 183) in the experimental mixture, which forms $C_8H_7O^-$ (m/z 119) by loss of SO_3 and readdition of $O_5^{.69}$ Figure 5c shows MS³ spectrum of C₁₈H₂₉O⁻ (m/z 261), which fragments by repeated loss of -CH2 (m/z 14) from the carbon chain, also yielding the C₈H₇O⁻ (m/z 119) fragment. While the fragmentations strongly suggest that $C_{18}H_{29}SO_3^-$ is similar to the DBSA standard, the MSⁿ experiments do not confirm the exact location and branching of the aliphatic carbon chain. As a result, it is concluded that C₁₈H₂₉SO₃ is an "Alkyl Benzene Sulfonatelike" (ABS-like) species. Similar MS² and MS³ patterns were

also observed for $C_{16}H_{25}SO_3^-$ (m/z 297) and $C_{15}H_{23}SO_3^-$ (m/z 283) ions, as shown in Figure S4. These fragmentation patterns match well with MSⁿ characteristics of DBSA and other sulfonic acid standards as illustrated by the bottom panels in Figure 5, indicating that these are also ABS-like species. Analogous MSⁿ patterns are also observed for $C_{18}H_{29}SO_4^-$ (m/z 341) ion summarized in Figure S5. The major MS² peak, $C_8H_7SO_4^-$ (m/z 199), fragments to form MS³ fragment $C_8H_7O_2^-$ (m/z 135). This same loss of m/z 64 is seen in other ABS-like species indicating that the parent ion $C_{18}H_{29}SO_4^-$ (m/z 341) is also a sulfonic acid, and the fourth oxygen molecule is attached to the carbon chain or benzene ring instead of being connected to the sulfur atom.

Overall, MSⁿ experiments with C₁₈H₂₉SO₃⁻ (*m/z* 325), C₁₆H₂₅SO₃⁻ (*m/z* 297), C₁₅H₂₃SO₃⁻ (*m/z* 283), and C₁₈H₂₉SO₄⁻ (*m/z* 341) produced fragmentation patterns very similar to that of the DBSA standard, which suggests that these components are all ABS-like species. To provide additional support to this conclusion, MSⁿ experiments of a commercial standard of Bis-(4-hydroxyphenyl)sulfone (BHPS), C₁₂H₉SO₄⁻ (*m/z* 249), an organic sulfone, are shown in contrast in Figure S6. BHPS fragmentation reported here also matches published literature for BHPS.⁷³ The MS² and MS³ fragmentation patterns identified in these experiments do not match fragmentation seen in any of the suspected ABS-like species, ruling out the possibility that the unusual RSO₃ species detected in this sample are sulfones.

Additional MSⁿ fragmentation experiments were employed for structural elucidation and identification of common organosulfate species in the sample. The formation of hydrogen sulfate ions (HSO₄⁻) (*m*/*z* 97) in MSⁿ experiments is a strong indicator of common organosulfates, and therefore can be employed to identify such species. With the exception of C₁₈H₂₉SO₄⁻ (*m*/*z* 341) discussed earlier, MSⁿ fragmentation of RSO₄⁻ indicates that these species are organosulfates. For example, MS² of C₁₂H₂₅SO₄⁻ (*m*/*z* 265) and of C₁₄H₂₉SO₄⁻ (*m*/*z* 293), shown in Figure S7, generate hydrogen sulfate ions, indicating that both species are organosulfates.

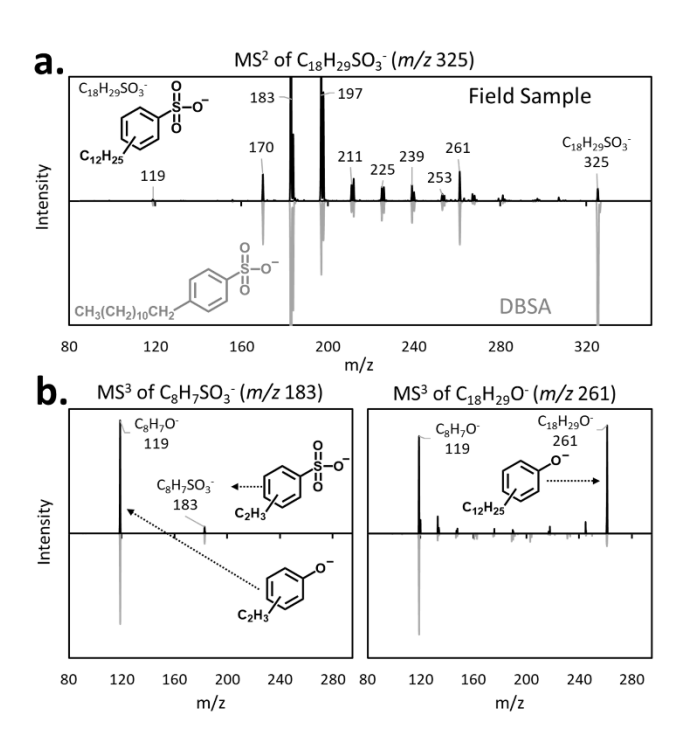


FIGURE 5. MSⁿ fragmentation of OS component $C_{18}H_{29}SO_3$ · m/z 325 (top, black), and commercial DBSA standard $C_{18}H_{29}SO_3$ · m/z 325 (bottom, grey) plotted for comparison to confirm the identity of ABS-like species. Panel (a) shows MS² fragmentation of both species. Panel (b) shows MS³ fragmentation of the m/z 183 fragment and panel (c) shows MS³ fragmentation of the m/z 261 fragment. Fragmentation patterns of commercial DBSA agree with published literature. $^{68-72}$

Figure 6 compares the molecular characteristics of each compound class in terms of their number of carbon atoms and aromaticity. Notably, CHO and CHON species have lower numbers of carbon atoms (#C<11, m/z<250); whereas CHOS compounds contain a larger number of carbon atoms (11<#C<23, m/z>250). These differences in molecular size between CHON and CHOS components are likely indicative of the atmospheric processes governing their formation. Specifically, single-ring nitroaromatic CHON compounds are low volatility condensedphase products of photochemical reactions between gas-phase volatile organic compounds (VOCs) and OH/NOx oxidant species.74 On the other hand, organosulfates and organosulfonates (CHOS) are generated through aqueous chemistry that occurs in aerosols when low-volatility dissolved organic species interact with sulfur-containing oxidants.75-77 To corroborate this hypothesis, we calculated the saturation mass concentrations of the CHO precursors that correspond to the observed CHON and CHOS products. The results were subsequently categorized into volatility bins for further analysis (Supplemental Note 4, Figure S8). The results reveal that the precursors of CHON primarily fall within the volatile and intermediate volatility bins (VOC and IVOC), consistent with their classification as atmospheric gas-phase components. Conversely, the precursors of CHOS predominantly occupy the semi-volatile and low volatility bins (SVOC and LVOC), aligning with their atmospheric condensed-phase tendency.

Figure 6b presents the double bond equivalent (DBE) values for the assigned species. Species which fall in the region between the 0.9×C limit⁷⁸ and the Linear Polyenes line⁷⁹ are substantially aromatic and are therefore likely BrC chromophores. The majority of CHO species with #C<11 and CHON species with #C+N≤8 fall within this region. It is likely that these species contribute to the overall BrC properties of the sampled OA. In contrast, CHOS species fall below the Linear Polyenes line, suggesting that they may not possess strong BrC properties. The low DBE values of CHOS species also indicate that they do not have a substantial degree of oxidation, which has been previously confirmed through structural characterization by MSⁿ. This suggests that the CHOS species have low BrC chromophore potential and they are likely not formed as a result of addition and condensation reactions with CHO or CHON species. Additionally, it has been shown that spontaneous oxidation of sulfones (-RSO₂) to sulfonic acids (-RSO₃) may occur on the surface of ESI droplets.80 Therefore, it is possible that the uncommon OS species detected by AMS are attributed to sulfones present in the wildfire smoke, and RSO₃ species detected by the HRMS may be formed through oxidation of the sulfones in the ESI droplets.

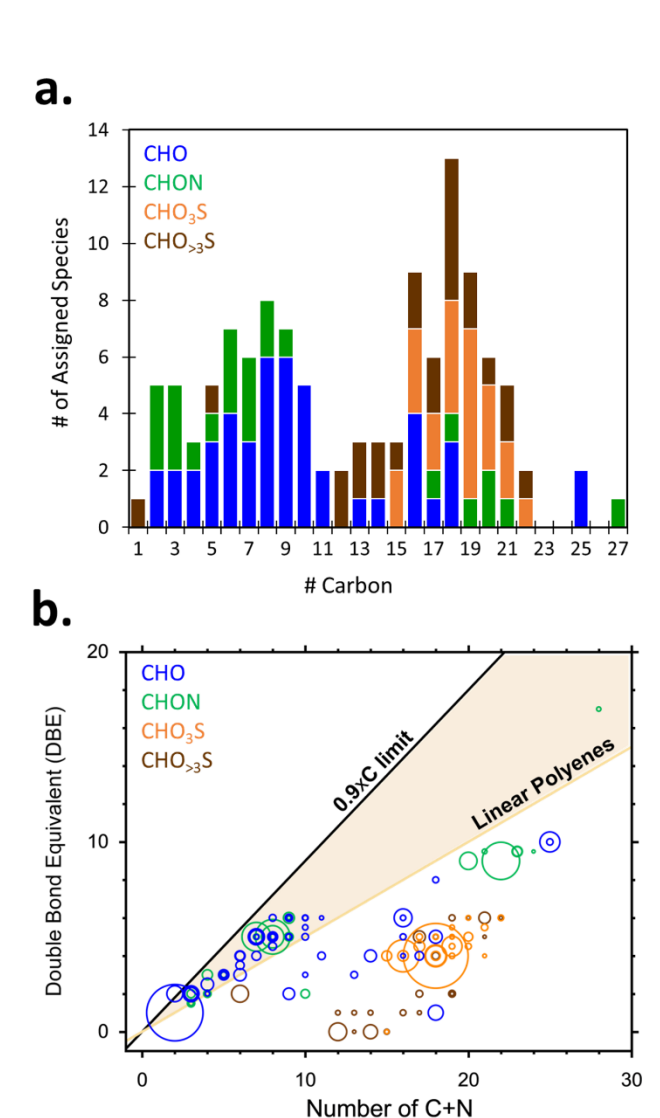


FIGURE 6. Composition characteristics of components identified in the OA sample extract. (a) Total count of identified species in each compound class, CHO (blue), CHON (green), CHO₃S (orange), and CHO_{>3}S (brown) plotted as a function of the number of carbon atoms. (b) Plot of the double bond equivalent (DBE) versus number of C+N atoms of assigned species. Size of the symbols is scaled to the cubic root of MS peak intensity. Reference lines show DBE references corresponding to linear polyenes⁷⁹ and 0.9×C unsaturation limit corresponding to fullerene-like hydrocarbons.⁷⁸ Species with C < 2 are removed for clarity. OS species containing adducts are grouped according to the compound class of their corresponding parent ion. The ABS-like RSO₄ species, $C_{18}H_{29}SO_{4}$, is grouped in the CHO₃S compound class.

Consistent with the observed trends depicted in the DBE plot of Figure 6b, further examination of HPLC-PDA data shown in Figure 7 reveals that \sim 44% of the BrC light-absorption is attributed to assigned CHO and CHON compounds. Figure 7 summarizes values of the mass absorption coefficient of the organic fraction (MAC_{OM}) collected on the filter, extracted, and subsequently analyzed by HPLC-PDA in the bulk-phase. The MAC_{OM} fractions attributed to CHO and CHON species are derived from the cumulative contributions of assigned species labelled in Figure S9. The MAC_{OM} fraction attributed to unassigned components includes contributions from prominent

light-absorbing features in the chromatogram that lack explicit identification. Additionally, the unresolved fraction includes additional light absorption that reflects contributions from minor unassigned regions within the chromatogram. Lastly, the unretained fraction encompasses the overall contribution of the material that eluted within 0-3 minutes. Specific details elaborating on the calculation of MAC_{OM} contributions are included in Supplementary Note 5. In previous studies employing similar analysis techniques, the MAC_{OM} values for laboratory-generated bulk-phase BrC were reported. West et al reported MACOC values in a range of 0.49-0.02 m²/g at 350 nm for BrC sampled from ethane flames with characteristic temperatures of 1946 K and 1863 K, respectively. 21 Hettiyadura et al reported a MACOM value of ~0.4 m²/g at 350 nm for BrC generated from heated wood pellets under pyrolysis conditions.²⁸ In our work here, MAC_{OM} at the same 350 nm is approximately 0.28 m²/g. Furthermore, MAC_{OM} values over an entire wavelength range of 300-450 nm reported here is consistently lower than those reported by Hettiyadura et al and West et al, indicating significantly less absorbing BrC properties of the organic material sampled in our present study. Additionally, it is important to note that the HPLC analysis exclusively covers the soluble organic fraction, as insoluble material is filtered by the column guard. Therefore, the injected OM mass assumed for the MAC_{OM} calculations (see Supplemental Note 5) may be overestimated, compared to what is actually being delivered to the PDA, causing an underestimation of the reported MAC_{OM} values.

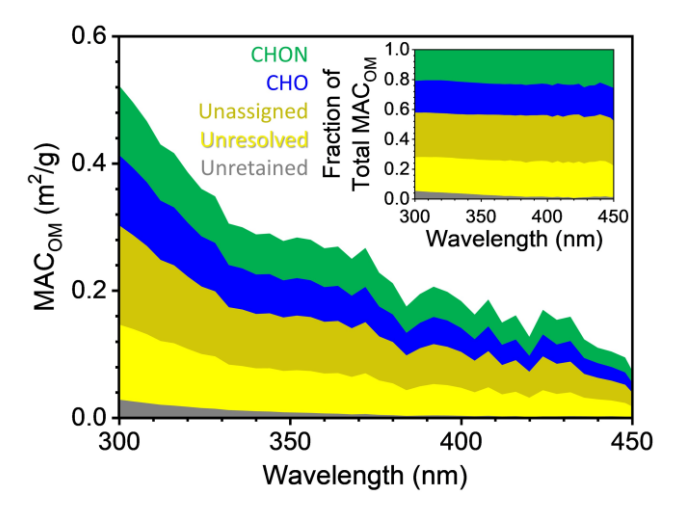


Figure 7. Light absorbing features of the August 3rd sample extract quantified as MAC (m²/g) values, fractionated to indicate contributions from different groups of OA constituents. The inset shows the distribution of the total MAC as a fraction from 0-1.

Molecular characterization of individual OA components obtained from HPLC-PDA-HRMS analysis guided interpretation of the time-resolved *in-situ* EESI-MS records. ¹⁸ Specifically, the aging profiles of selected individual OA species, identified in the offline HPLC-HRMS analysis, were retrieved from the EESI-MS data. The time-resolved EESI-MS records were successfully retrieved for the following OA species: C₃H₄O₃, C₇H₆O₂, C₇H₆O₃, C₁₈H₃₆O₃, C₆H₅NO₃, C₆H₅NO₄, C₇H₇NO₄, C₁₂H₂₆SO₄, C₁₆H₂₆SO₃, C₇H₆N₂O₆, C₁₄H₃₀SO₄, C₁₄H₃₀SO₅, C₁₆H₂₄SO₃, C₁₇H₂₈SO₄, C₁₅H₂₄SO₃, and C₁₅H₃₂SO₃ (all listed as neutral species). As shown in Figure 4, each of these OA species retrieved by EESI-MS, displayed one to three major HPLC-

HRMS elution peaks. Figure 8a shows a representative timeresolved EESI-MS record of a [M-H] ion corresponding to C₁₂H₂₆SO₄ species, plotted together with the CO record as a function of the flight time. All other aging profiles retrieved from the EESI-MS records are included in the SI (Figures S10-S12). The data collected from 10:15 PM to 12:15 AM UTC represent the first period of transecting the biomass burning emissions plume originating from the source and travelling downwind (Figure 1). 12:15 AM to 2:15 AM represents the second period of transecting the smoke plume following a similar trajectory. The observed maxima in each period occur when the aircraft transects the middle of the plume, and the minima are the baseline values measured outside the plume. To account for plume dilution downwind of the wildfire, changes in the EESI-MS signals from individual OA species are compared with changes in the CO signal. The blue triangles represent the ratio of $\Delta [C_{12}H_{25}SO_4]/\Delta [CO]$ averaged across each plume transect to show the trending change in the ratio. A linear fit line of these ratios is plotted for each of the two periods to facilitate visualization of the aging profile, while accounting for plume dilution. Figure 8b shows in-plume ratios of $\Delta [C_{12}H_{25}SO_4]/\Delta [CO]$ plotted as a function of physical smoke age, which was calculated by fitting the data as a function of exponential decay. The difference, Δ, values used in the ratios of C₁₂H₂₅SO₄ and CO were determined by subtracting the 'background' concentrations from the 'in-plume' concentrations during each pass across the plume. 'Background' concentrations were averaged over 60 s time intervals both before and after each plume transect, and 'in-plume' concentrations were averaged across the entire plume transect. The obtained data points are color-coded according to the total OA mass measured by AMS.

The half-life of C₁₂H₂₅SO₄ in the plume was then calculated from a first-order exponential decay fit of $\Delta [C_{12}H_{26}SO_4]/\Delta [CO]$ versus characteristic time of the physical smoke age, as illustrated in Fig 8b. Figure 8c summarizes half-life times of all individual species identified by the HPLC-PDA-HRMS analysis for which the EESI-MS time-resolved records were successfully retrieved (listed as neutral species). With respect to their in-plume aging behavior, two groups of species were observed: i) aging-susceptible, rapidly decaying species with half-life times of 1-2.5 hours, and ii) aging-resilient species that did not show detectable changes on the time scale of the field experiment (~8 hours). CHO and most of the CHON species were aging-susceptible, while the majority of the CHOS species showed aging-resilient characteristics. This suggests that CHOS compounds may be more stable than CHO and CHON; however, more individual species should be systematically investigated to provide conclusive and comprehensive information on the aging kinetics and evolution of the individual OA constituents in each class of compounds. Additionally, investigation of the emission rates of organosulfur compounds is also needed to separate any potential shifts in emissions that could confound the aging analysis presented here. The presented complementary applications of offline HPLC-HRMS and online EESI-MS analytical techniques enable unique chemical speciation of the individual components within a complex OA matrix, providing their in-depth chemical description and assessing their aging transformations.

CONCLUSIONS. The complementary use of airborne measurements by AMS and EESI-MS, along with offline HPLC-PDA-ESI-HRMS and tandem MSⁿ measurements, is presented

here as a novel multi-modal method for investigating wildfire BBOA. This integrated approach provides a comprehensive understanding of the aging characteristics of individual molecular components. In essence, AMS provides quantitative measurements of broad classes of OA, which guides in-depth HRMS analysis of individual molecular components. In turn, the HRMS data informs interpretation of time-resolved EESI profiles, enabling us to elucidate the fate of individual species. Through AMS analysis, we have identified substantial presence of OS in the wildfire sample, which led to further investigation of OS species by HRMS and tandem MS, revealing the presence of uncommon ABS-like species. Additionally, we identified common organo-sulfates, nitroaromatics, and oxygenated aromatics, frequently found in BBOA samples.

Finally, by employing these multi-modal MS techniques, we successfully decipher aging trends of individual species in real-world complex mixtures of OA. We observed the decay of more reactive OA components within approximately 3 hours, while more stable OA components persist in the atmosphere for more than 8 hours. These aging characteristics are difficult to predict due to the complexity and variability of atmospheric OA, ¹¹ and due to the variety of chemical and physical processes that contribute both to the formation and loss of OA. ^{81,82} Therefore, the application of time-resolved AMS and EESI, along with offline HRMS analyses, provides essential information to gain insights into the formation and fate of specific BBOA, which impacts climate, atmospheric chemistry, and human health.

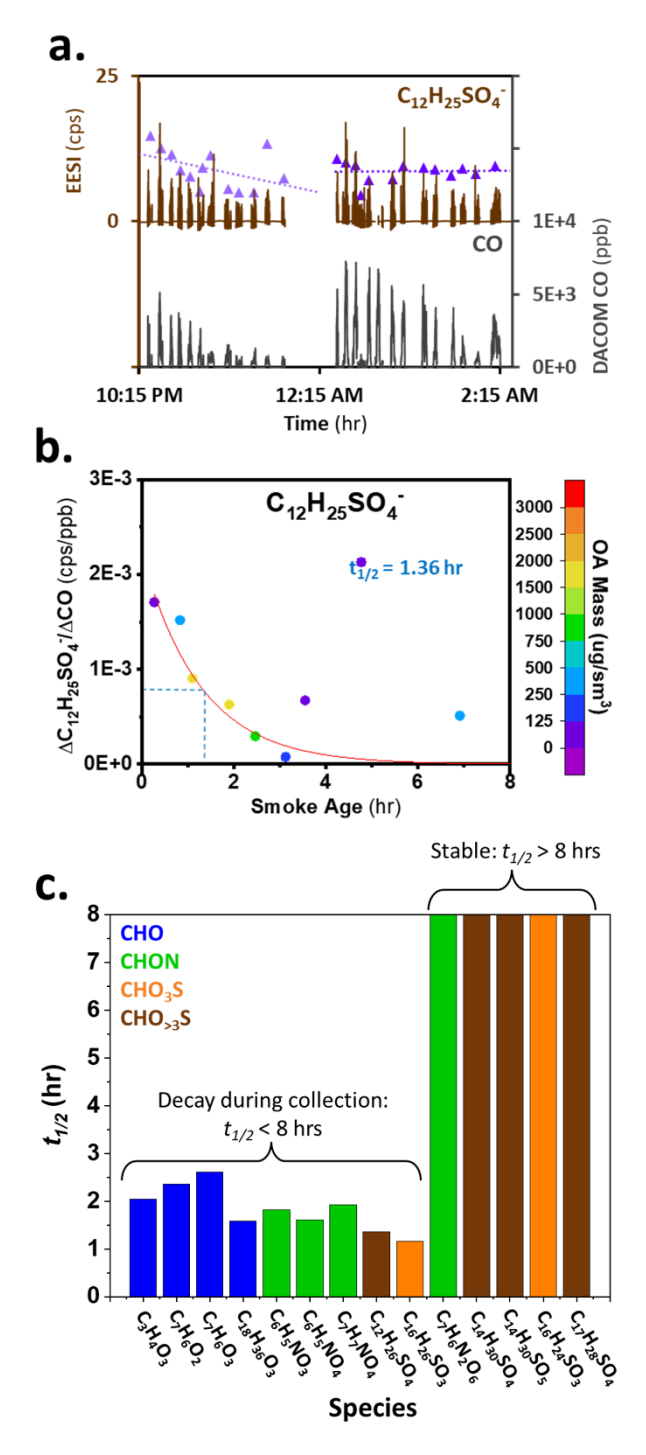


FIGURE 8. (a) EESI-MS time-resolved records of $C_{12}H_{25}SO_4^-$ and CO as a function of flight time (UTC). The 'in-plume' ratios of $\Delta[C_{12}H_{25}SO_4^-]/\Delta[CO]$ are plotted for the 1^{st} full pass (light purple) and 2^{nd} full pass (dark purple) as a function of flight time. (b) 'In-plume' ratios of $\Delta[C_{12}H_{25}SO_4^-]/\Delta[CO]$ are plotted with respect to the time of smoke age, color-coded according to total OA mass of the sample at a given time. Formal first-order reaction kinetics are used to fit the data and estimate half-life time of $C_{12}H_{26}SO_4$ in the plume. (c) Summary of the half-life times of major species investigated. Additional plots of the major species investigated by EESI-MS are included in SI file, Figures S10-S12.

ASSOCIATED CONTENT

Supporting Information

The Supporting Information is available free of charge on the ACS Publications website.

Supporting Information including supplementary notes on field deployment, summary of HRMS analysis, summary of tandem MS experiments, optical data and classification, and summary of EESI analysis is available on PDF.

AUTHOR INFORMATION

Corresponding Author

Alexander Laskin – Department of Chemistry, Department of Earth, Atmospheric & Planetary Sciences, Purdue University, West Lafayette, Indiana 47907, USA orcid.org/0000-0002-7836-8417; Email: alaskin@purdue.edu

Author Contributions

K.S. and A.L. designed the overall project framework and manuscript logic. K.S. performed the HPLC-PDA-HRMS molecular characterization experiments and led data analysis and data integration tasks with assistance from D.P., H.G. and PC-J. D.P., H.G., M.S., J.J. and P. C.-J. deployed AMS and EESI-MS onboard research aircraft, performed real-time measurements, and collected aerosol samples. J.D. deployed SAGA-MC-IC and collected and extracted additional aerosol samples to quantify water-soluble ions. K.S. and A.L. integrated the experimental datasets and wrote the manuscript, and all authors contributed in its review and editing. J.J. and A.L. secured grant support for this study and managed the project.

Notes

Any additional relevant notes should be placed here.

ACKNOWLEDGMENT

Purdue University group acknowledge partial support from U.S. Department of Energy's Atmospheric System Research Program, Office of Biological and Environmental Research (grant DESC0018948) and from the National Science Foundation (grant AGS-2039985). The University of Colorado group acknowledges NASA grants 80NSSC21K1451 and 80NSSC18K0630. FIREXAQ is a large-scale field study of wildfires and agricultural fires across the United States, led by National Oceanic and Atmospheric Administration and National Aeronautics and Space Administration. We acknowledge Glenn Diskin from NASA Langley for use of the CO data.

REFERENCES

(1) Hallquist, M.; Wenger, J. C.; Baltensperger, U.; Rudich, Y.; Simpson, D.; Claeys, M.; Dommen, J.; Donahue, N. M.; George, C.; Goldstein, A. H.; Hamilton, J. F.; Herrmann, H.; Hoffmann, T.; Iinuma, Y.; Jang, M.; Jenkin, M. E.; Jimenez, J. L.; Kiendler-Scharr, A.; Maenhaut, W.; McFiggans, G.; Mentel, T. F.; Monod, A.; Prévôt, A. S. H.; Seinfeld, J. H.; Surratt, J. D.; Szmigielski, R.; Wildt, J. The Formation, Properties and Impact of Secondary

- Organic Aerosol: Current and Emerging Issues. *Atmospheric Chemistry and Physics* **2009**, *9* (14), 5155–5236. https://doi.org/10.5194/acp-9-5155-2009.
- (2) Shrivastava, M.; Cappa, C. D.; Fan, J.; Goldstein, A. H.; Guenther, A. B.; Jimenez, J. L.; Kuang, C.; Laskin, A.; Martin, S. T.; Ng, N. L.; Petaja, T.; Pierce, J. R.; Rasch, P. J.; Roldin, P.; Seinfeld, J. H.; Shilling, J.; Smith, J. N.; Thornton, J. A.; Volkamer, R.; Wang, J.; Worsnop, D. R.; Zaveri, R. A.; Zelenyuk, A.; Zhang, Q. Recent Advances in Understanding Secondary Organic Aerosol: Implications for Global Climate Forcing. Reviews of Geophysics 2017, 55 (2), 509–559.

https://doi.org/10.1002/2016RG000540.

- (3) Jimenez, J. L.; Canagaratna, M. R.; Donahue, N. M.; Prevot, A. S. H.; Zhang, Q.; Kroll, J. H.; DeCarlo, P. F.; Allan, J. D.; Coe, H.; Ng, N. L.; Aiken, A. C.; Docherty, K. S.; Ulbrich, I. M.; Grieshop, A. P.; Robinson, A. L.; Duplissy, J.; Smith, J. D.; Wilson, K. R.; Lanz, V. A.; Hueglin, C.; Sun, Y. L.; Tian, J.; Laaksonen, A.; Raatikainen, T.; Rautiainen, J.; Vaattovaara, P.; Ehn, M.; Kulmala, M.; Tomlinson, J. M.; Collins, D. R.; Cubison, M. J.; E.; Dunlea, J.; Huffman, J. A.; Onasch, T. B.; Alfarra, M. R.; Williams, P. I.; Bower, K.; Kondo, Y.; Schneider, J.; Drewnick, F.; Borrmann, S.; Weimer, S.; Demerjian, K.; Salcedo, D.; Cottrell, L.: Griffin, R.: Takami, A.: Mivoshi, T.; Hatakeyama, S.; Shimono, A.; Sun, J. Y.; Zhang, Y. M.; Dzepina, K.; Kimmel, J. R.; Sueper, D.; Jayne, J. T.; Herndon, S. C.; Trimborn, A. M.; Williams, L. R.; Wood, E. C.; Middlebrook, A. M.; Kolb, C. E.; Baltensperger, U.; Worsnop, D. R. Evolution of Organic Aerosols in the Atmosphere. Sci-2009. *326* (5959), 1525–1529. ence https://doi.org/10.1126/science.1180353.
- (4) Zhang, Q.; Jimenez, J. L.; Canagaratna, M. R.; Ulbrich, I. M.; Ng, N. L.; Worsnop, D. R.; Sun, Y. Understanding Atmospheric Organic Aerosols via Factor Analysis of Aerosol Mass Spectrometry: A Review. *Anal Bioanal Chem* 2011, 401 (10), 3045–3067. https://doi.org/10.1007/s00216-011-5355-y.

- (5) Andreae, M. O. Emission of Trace Gases and Aerosols from Biomass Burning an Updated Assessment. *Atmospheric Chemistry and Physics* **2019**, *19* (13), 8523–8546. https://doi.org/10.5194/acp-19-8523-2019.
- Kanakidou, M.; Seinfeld, J. H.; Pandis, S. N.; Barnes, I.; Dentener, F. J.; Facchini, M. C.; Van Dingenen, R.; Ervens, B.; Nenes, A.; Nielsen, C. J.; Swietlicki, E.; Putaud, J. P.; Balkanski, Y.; Fuzzi, S.; Horth, J.; Moortgat, G. K.; Winterhalter, R.; Myhre, C. E. L.; Tsigaridis, K.; Vignati, E.; Stephanou, E. G.; Wilson, J. Organic Aerosol and Global Climate Modelling: A Review. *Atmospheric Chemistry and Physics* 2005, 5 (4), 1053–1123. https://doi.org/10.5194/acp-5-1053-2005.
- **(7)** Boucher, O.; Randall, D.; Artaxo, P.; Bretherton, C.; Feingold, G.; Forster, P.; Kerminen, V.-M.; Kondo, Y.; Liao, H.; Lohmann, U.; Rasch, P.; Satheesh, S. K.; Sherwood, S.; Stevens, B.; Zhang, X. Y. 2013: Clouds and Aerosols. IPCC, 2013: Climate Change 2013: The Physical Science Basis. Contribution of Working Group I to the Fifth Assessment Report of the Intergovernmental Panel on Climate Change; Stocker, T. F., Qin, D., Plattner, G.-K., Tignor, M., Allen, S. K., Boschung, J., Nauels, A., Xia, Y., Bex, V., Midgley, P. M., Eds.; Cambridge University Press: Cambridge, United Kingdom and New York, NY, USA, 2007.
- (8) McNeill, V. F. Atmospheric Aerosols: Clouds, Chemistry, and Climate. *Annu. Rev. Chem. Biomol.* **2017**, *8* (1), 427–444. https://doi.org/10.1146/annurev-chembioeng-060816-101538.
- (9) Andreae, M. O.; Rosenfeld, D. Aerosol–Cloud–Precipitation Interactions. Part 1. The Nature and Sources of Cloud-Active Aerosols. *Earth-Science Reviews* **2008**, *89* (1), 13–41. https://doi.org/10.1016/j.earscirev.2008.03.001.
- (10) Knopf, D. A.; Alpert, P. A.; Wang, B. The Role of Organic Aerosol in Atmospheric Ice Nucleation: A Review. *ACS Earth and Space Chemistry* **2018**, *2* (3), 168–202. https://doi.org/10.1021/acsearthspace-chem.7b00120.

- (11) Moise, T.; Flores, J. M.; Rudich, Y. Optical Properties of Secondary Organic Aerosols and Their Changes by Chemical Processes. *Chem. Rev.* **2015**, *115* (10), 4400–4439. https://doi.org/10.1021/cr5005259.
- (12) Laskin, A.; Laskin, J.; Nizkorodov, S. A. Chemistry of Atmospheric Brown Carbon. *Chem. Rev.* **2015**, *115* (10), 4335–4382. https://doi.org/10.1021/cr5006167.
- (13) Wang, X.; Heald, C. L.; Liu, J.; Weber, R. J.; Campuzano-Jost, P.; Jimenez, J. L.; Schwarz, J. P.; Perring, A. E. Exploring the Observational Constraints on the Simulation of Brown Carbon. *Atmos. Chem. Phys.* **2018**, *18* (2), 635–653. https://doi.org/10.5194/acp-18-635-2018.
- (14) Zhang, A.; Wang, Y.; Zhang, Y.; Weber, R. J.; Song, Y.; Ke, Z.; Zou, Y. Modeling the Global Radiative Effect of Brown Carbon: A Potentially Larger Heating Source in the Tropical Free Troposphere than Black Carbon. Atmospheric Chemistry and Physics 2020, 20 (4), 1901–1920. https://doi.org/10.5194/acp-20-1901-2020.
- (15) Pöschl, U. Atmospheric Aerosols: Composition, Transformation, Climate and Health Effects. *Angewandte Chemie International Edition* **2005**, *44* (46), 7520–7540. https://doi.org/10.1002/anie.200501122.
- (16) Schueneman, M. K.; Nault, B. A.; Campuzano-Jost, P.; Jo, D. S.; Day, D. A.; Schroder, J. C.; Palm, B. B.; Hodzic, A.; Dibb, J. E.; Jimenez, J. L. Aerosol pH Indicator and Organosulfate Detectability from Aerosol Mass Spectrometry Measurements. *Atmospheric Measurement Techniques* **2021**, 14 (3), 2237–2260. https://doi.org/10.5194/amt-14-2237-2021.
- (17) Guo, H.; Campuzano-Jost, P.; Nault, B. A.; Day, D. A.; Schroder, J. C.; Kim, D.; Dibb, J. E.; Dollner, M.; Weinzierl, B.; Jimenez, J. L. The Importance of Size Ranges in Aerosol Instrument Intercomparisons: A Case Study for the Atmospheric Tomography Mission. *Atmospheric Measurement Techniques* **2021**, *14* (5), 3631–3655. https://doi.org/10.5194/amt-14-3631-2021.
- (18) Pagonis, D.; Campuzano-Jost, P.; Guo, H.; Day, D. A.; Schueneman, M. K.; Brown, W. L.; Nault, B. A.; Stark, H.; Siemens, K.;

- Laskin, A.; Piel, F.; Tomsche, L.; Wisthaler, A.; Coggon, M. M.; Gkatzelis, G. I.; Halliday, H. S.; Krechmer, J. E.; Moore, R. H.; Thomson, D. S.; Warneke, C.; Wiggins, E. B.; Jimenez, J. L. Airborne Extractive Electrospray Mass Spectrometry Measurements of the Chemical Composition of Organic Aerosol. *Atmospheric Measurement Techniques* **2021**, *14* (2), 1545–1559. https://doi.org/10.5194/amt-14-1545-2021.
- (19) DeCarlo, P. F.; Kimmel, J. R.; Trimborn, A.; Northway, M. J.; Jayne, J. T.; Aiken, A. C.; Gonin, M.; Fuhrer, K.; Horvath, T.; Docherty, K. S.; Worsnop, D. R.; Jimenez, J. L. Field-Deployable, High-Resolution, Time-of-Flight Aerosol Mass Spectrometer. *Anal. Chem.* 2006, 78 (24), 8281–8289. https://doi.org/10.1021/ac061249n.
- (20) Lin, P.; Fleming, L. T.; Nizkorodov, S. A.; Laskin, J.; Laskin, A. Comprehensive Molecular Characterization of Atmospheric Brown Carbon by High Resolution Mass Spectrometry with Electrospray and Atmospheric Pressure Photoionization. *Anal. Chem.* **2018**, *90* (21), 12493–12502. https://doi.org/10.1021/acs.anal-chem.8b02177.
- (21) West, C. P.; Hettiyadura, A. P. S.; Darmody, A.; Mahamuni, G.; Davis, J.; Novosselov, I.; Laskin, A. Molecular Composition and the Optical Properties of Brown Carbon Generated by the Ethane Flame. *ACS Earth Space Chem.* **2020**, *4* (7), 1090–1103. https://doi.org/10.1021/acsearthspacechem.0c00095.
- (22) Lin, P.; Liu, J.; Shilling, J. E.; Kathmann, S. M.; Laskin, J.; Laskin, A. Molecular Characterization of Brown Carbon (BrC) Chromophores in Secondary Organic Aerosol Generated from Photo-Oxidation of Toluene. *Phys. Chem. Chem. Phys.* **2015**, *17* (36), 23312–23325. https://doi.org/10.1039/C5CP02563J.
- (23) Montoya-Aguilera, J.; Horne, J. R.; Hinks, M. L.; Fleming, L. T.; Perraud, V.; Lin, P.; Laskin, A.; Laskin, J.; Dabdub, D.; Nizkorodov, S. A. Secondary Organic Aerosol from Atmospheric Photooxidation of Indole. *Atmos. Chem. Phys.* **2017**, *17* (18),

- 11605–11621. https://doi.org/10.5194/acp-17-11605-2017.
- (24) Laskin, A.; Lin, P.; Laskin, J.; Fleming, L. T.; Nizkorodov, S. Molecular Characterization of Atmospheric Brown Carbon. *Multiphase Environmental Chemistry in the Atmosphere*, ACS **2018**, 1299, 261–274.
- (25) Lin, P.; Aiona, P. K.; Li, Y.; Shiraiwa, M.; Laskin, J.; Nizkorodov, S. A.; Laskin, A. Molecular Characterization of Brown Carbon in Biomass Burning Aerosol Particles. *Environ. Sci. Technol.* **2016**, *50* (21), 11815–11824. https://doi.org/10.1021/acs.est.6b03024.
- (26) Li, C.; He, Q.; Hettiyadura, A. P. S.; Kaf, U.; Meidan, D.; Zimmermann, R.; Brown, S. S.; George, C.; Laskin, A.; Rudich, Y. Formation of Secondary Brown Carbon in Biomass Burning Aerosol Proxies through NO3 Radical Reactions. *Environ. Sci. Technol.* 2020, 54 (3), 1395–1405. https://doi.org/10.1021/acs.est.9b05641.
- (27) Fleming, L. T.; Lin, P.; Roberts, J. M.; Selimovic, V.; Yokelson, R.; Laskin, J.; Laskin, A.; Nizkorodov, S. A. Molecular Composition and Photochemical Lifetimes of Brown Carbon Chromophores in Biomass Burning Organic Aerosol. *Atmos. Chem. Phys.* **2020**, *20* (2), 1105–1129. https://doi.org/10.5194/acp-20-1105-2020.
- (28) Hettiyadura, A. P. S.; Garcia, V.; Li, C.; West, C. P.; Tomlin, J.; He, Q.; Rudich, Y.; Laskin, A. Chemical Composition and Molecular-Specific Optical Properties of Atmospheric Brown Carbon Associated with Biomass Burning. *Environ. Sci. Technol.* **2021**, 55 (4), 2511–2521. https://doi.org/10.1021/acs.est.0c05883.
- (29) Warneke, C.; Schwarz, J. P.; Dibb, J.; Kalashnikova, O.; Frost, G.; Al-Saad, J.; Brown, S. S.; Brewer, Wm. A.; Soja, A.; Seidel, F. C.; Washenfelder, R. A.; Wiggins, E. B.; Moore, R. H.; Anderson, B. E.; Jordan, C.; Yacovitch, T. I.; Herndon, S. C.; Liu, S.; Kuwayama, T.; Jaffe, D.; Johnston, N.; Selimovic, V.; Yokelson, R.; Giles, D. M.; Holben, B. N.; Goloub, P.; Popovici, I.; Trainer, M.; Kumar, A.; Pierce, R. B.; Fahey, D.; Roberts, J.; Gargulinski, E. M.; Peterson, D. A.; Ye, X.; Thapa, L. H.;

- Saide, P. E.; Fite, C. H.; Holmes, C. D.; Wang, S.; Coggon, M. M.; Decker, Z. C. J.; Stockwell, C. E.; Xu, L.; Gkatzelis, G.; Aikin, K.; Lefer, B.; Kaspari, J.; Griffin, D.; Zeng, L.; Weber, R.; Hastings, M.; Chai, J.; Wolfe, G. M.; Hanisco, T. F.; Liao, J.; Campuzano Jost, P.; Guo, H.; Jimenez, J. L.; Crawford, J.; Team, T. F.-A. S. Fire Influence on Regional to Global Environments and Air Quality (FIREX-AQ). *Journal of Geophysical Research: Atmospheres* **2023**, 128 (2), e2022JD037758. https://doi.org/10.1029/2022JD037758.
- (30) Canagaratna, M. r.; Jayne, J. t.; Jimenez, J. l.; Allan, J. d.; Alfarra, M. r.; Zhang, Q.; Onasch, T. b.; Drewnick, F.; Coe, H.; Middlebrook, A.; Delia, A.; Williams, L. r.; Trimborn, A. m.; Northway, M. j.; DeCarlo, P. f.; Kolb, C. e.; Davidovits, P.; Worsnop, D. r. Chemical and Microphysical Characterization of Ambient Aerosols with the Aerodyne Aerosol Mass Spectrometer. *Mass Spectrometry Reviews* **2007**, *26* (2), 185–222. https://doi.org/10.1002/mas.20115.
- (31) Lopez-Hilfiker, F. D.; Pospisilova, V.; Huang, W.; Kalberer, M.; Mohr, C.; Stefenelli, G.; Thornton, J. A.; Baltensperger, U.; Prevot, A. S. H.; Slowik, J. G. An Extractive Electrospray Ionization Time-of-Flight Mass Spectrometer (EESI-TOF) for Online Measurement of Atmospheric Aerosol Particles. *Atmospheric Measurement Techniques* **2019**, *12* (9), 4867–4886.
- (32) Chen, H.; Venter, A.; Cooks, R. G. Extractive Electrospray Ionization for Direct Analysis of Undiluted Urine, Milk and Other Complex Mixtures without Sample Preparation. *Chem. Commun.* **2006**, No. 19, 2042–2044. https://doi.org/10.1039/b602614a.

https://doi.org/10.5194/amt-12-4867-2019.

(33) Doezema, L. A.; Longin, T.; Cody, W.; Perraud, V.; Dawson, M. L.; Ezell, M. J.; Greaves, J.; Johnson, K. R.; Finlayson-Pitts, B. J. Analysis of Secondary Organic Aerosols in Air Using Extractive Electrospray Ionization Mass Spectrometry (EESI-MS). *RSC Adv.* **2012**, *2* (7), 2930–2938. https://doi.org/10.1039/c2ra00961g.

- (34)Surdu, M.; Pospisilova, V.; Xiao, M.; Wang, M.; Mentler, B.; Simon, M.; Stolzenburg, D.; Hoyle, C. R.; Bell, D. M.; Lee, C. P.; Lamkaddam, H.; Lopez-Hilfiker, F.; Ahonen, L. R.; Amorim, A.; Baccarini, A.; Chen, D.; Dada, L.; Duplissy, J.; Finkenzeller, H.; He, X.-C.; Hofbauer, V.; Kim, C.; Kürten, A.; Kvashnin, A.; Lehtipalo, K.; Makhmutov, V.; Molteni, U.; Nie, W.; Onnela, A.; Petäjä, T.; Quéléver, L. L. J.; Tauber, C.; Tomé, A.; Wagner, R.; Yan, C.; Prevot, A. S. H.; Dommen, J.; Donahue, N. M.; Hansel, A.; Curtius, J.; Winkler, P. M.; Kulmala, M.; Volkamer, R.; Flagan, R. C.; Kirkby, J.; Worsnop, D. R.; Slowik, J. G.; Wang, D. S.; Baltensperger, U.; Haddad, I. el. Molecular Characterization of Ultrafine Particles Using Extractive Electrospray Time-of-Flight Mass Spectrome-Sci.: try. Environ. Atmos. 2021. https://doi.org/10.1039/D1EA00050K.
- (35) Gallimore, P. J.; Kalberer, M. Characterizing an Extractive Electrospray Ionization (EESI) Source for the Online Mass Spectrometry Analysis of Organic Aerosols. *Environ. Sci. Technol.* **2013**, *47* (13), 7324–7331. https://doi.org/10.1021/es305199h.
- (36) Gallimore, P. J.; Griffiths, P. T.; Pope, F. D.; Reid, J. P.; Kalberer, M. Comprehensive Modeling Study of Ozonolysis of Oleic Acid Aerosol Based on Real-Time, Online Measurements of Aerosol Composition. *Journal of Geophysical Research: Atmospheres* **2017**, *122* (8), 4364–4377. https://doi.org/10.1002/2016JD026221.
- (37) Liu, X.; Day, D. A.; Krechmer, J. E.; Brown, W.; Peng, Z.; Ziemann, P. J.; Jimenez, J. L. Direct Measurements of Semi-Volatile Organic Compound Dynamics Show near-Unity Mass Accommodation Coefficients for Diverse Aerosols. *Communications Chemistry* **2019**, *2* (1), 98. https://doi.org/10.1038/s42004-019-0200-x.
- (38) Liu, Q.; Liggio, J.; Wu, D.; Saini, A.; Halappanavar, S.; Wentzell, J. J. B.; Harner, T.; Li, K.; Lee, P.; Li, S.-M. Experimental Study of OH-Initiated Heterogeneous Oxidation of Organophosphate Flame Retardants: Kinetics, Mechanism, and Toxicity.

- Environ. Sci. Technol. **2019**, 53 (24), 14398–14408. https://doi.org/10.1021/acs.est.9b05327.
- (39) Brown, W. L.; Day, D. A.; Stark, H.; Pagonis, D.; Krechmer, J. E.; Liu, X.; Price, D. J.; Katz, E. F.; DeCarlo, P. F.; Masoud, C. G.; Wang, D. S.; Ruiz, L. H.; Arata, C.; Lunderberg, D. M.; Goldstein, A. H.; Farmer, D. K.; Vance, M. E.; Jimenez, J. L. Real-Time Organic Aerosol Chemical Speciation in the Indoor Environment Using Extractive Electrospray Ionization Mass Spectrometry. *Indoor Air* **2021**, *31* (1), 141–155. https://doi.org/10.1111/ina.12721.
- (40) Qi, L.; Chen, M.; Stefenelli, G.; Pospisilova, V.; Tong, Y.; Bertrand, A.; Hueglin, C.; Ge, X.; Baltensperger, U.; Prévôt, A. S. H.; Slowik, J. G. Organic Aerosol Source Apportionment in Zurich Using an Extractive Electrospray Ionization Timeof-Flight Mass Spectrometer (EESI-TOF-MS) Part 2: Biomass Burning Influences in Winter. *Atmospheric Chemistry and Physics* **2019**, *19* (12), 8037–8062. https://doi.org/10.5194/acp-19-8037-2019.
- (41) Stefenelli, G.; Pospisilova, V.; Lopez-Hilfiker, F. D.; Daellenbach, K. R.; Hüglin, C.; Tong, Y.; Baltensperger, U.; Prévôt, A. S. H.; Slowik, J. G. Organic Aerosol Source Apportionment in Zurich Using an Extractive Electrospray Ionization Time-of-Flight Mass Spectrometer (EESI-TOF-MS) Part 1: Biogenic Influences and Day–Night Chemistry in Summer. *Atmospheric Chemistry and Physics* **2019**, *19* (23), 14825–14848. https://doi.org/10.5194/acp-19-14825-2019.
- (42) Rickly, P. S.; Guo, H.; Campuzano-Jost, P.; Jimenez, J. L.; Wolfe, G. M.; Bennett, R.; Bourgeois, I.; Crounse, J. D.; Dibb, J. E.; DiGangi, J. P.; Diskin, G. S.; Dollner, M.; Gargulinski, E. M.; Hall, S. R.; Halliday, H. S.; Hanisco, T. F.; Hannun, R. A.; Liao, J.; Moore, R.; Nault, B. A.; Nowak, J. B.; Peischl, J.; Robinson, C. E.; Ryerson, T.; Sanchez, K. J.; Schöberl, M.; Soja, A. J.; St. Clair, J. M.; Thornhill, K. L.; Ullmann, K.; Wennberg, P. O.; Weinzierl, B.; Wiggins, E. B.; Winstead, E. L.; Rollins, A. W.

- Emission Factors and Evolution of SO₂ Measured from Biomass Burning in Wildfires and Agricultural Fires. *Atmospheric Chemistry and Physics* **2022**, *22* (23), 15603–15620. https://doi.org/10.5194/acp-22-15603-2022.
- (43)Saide, P. E.; Thapa, L. H.; Ye, X.; Pagonis, D.; Campuzano-Jost, P.; Guo, H.; Schuneman, M. L.; Jimenez, J.-L.; Moore, R.; Wiggins, E.; Winstead, E.; Robinson, C.; Thornhill, L.; Sanchez, K.; Wagner, N. L.; Ahern, A.; Katich, J. M.; Perring, A. E.; Schwarz, J. P.; Lyu, M.; Holmes, C. D.; Hair, J. W.; Fenn, M. A.; Shingler, T. J. Understanding the Evolution of Smoke Mass Extinction Efficiency Using Field Campaign Measurements. Geophysical Research Letters 2022, 49 (18),e2022GL099175.
 - https://doi.org/10.1029/2022GL099175.
- (44) Dibb, J. E.; Talbot, R. W.; Seid, G.; Jordan, C.; Scheuer, E.; Atlas, E.; Blake, N. J.; Blake, D. R. Airborne Sampling of Aerosol Particles: Comparison between Surface Sampling at Christmas Island and P-3 Sampling during PEM-Tropics B. *J. Geophys. Res.* **2002**, *108* (D2), 8230. https://doi.org/10.1029/2001JD000408.
- (45) Scheuer, E.; Talbot, R. W.; Dibb, J. E.; Seid, G. K.; DeBell, L.; Lefer, B. Seasonal Distributions of Fine Aerosol Sulfate in the North American Arctic Basin during TOPSE. *Journal of Geophysical Research: Atmospheres* **2003**, *108* (D4). https://doi.org/10.1029/2001JD001364.
- (46) Cofer, W. R.; Collins, V. G.; Talbot, R. W. Improved Aqueous Scrubber for Collection of Soluble Atmospheric Trace Gases. *Environ. Sci. Technol.* **1985**, *19* (6), 557–560. https://doi.org/10.1021/es00136a012.
- (47) Cofer, W. R.; Edahl, R. A. A New Technique for Collection, Concentration and Determination of Gaseous Tropospheric Formaldehyde. *Atmospheric Environment* (1967) 1986, 20 (5), 979–984. https://doi.org/10.1016/0004-6981(86)90282-9.
- (48) Spaulding, R. S.; Talbot, R. W.; Charles, M. J. Optimization of a Mist Chamber (Cofer Scrubber) for Sampling Water-Soluble

- Organics in Air. *Environ. Sci. Technol.* **2002**, *36* (8), 1798–1808. https://doi.org/10.1021/es011189x.
- (49) Pluskal, T.; Castillo, S.; Villar-Briones, A.; Orešič, M. MZmine 2: Modular Framework for Processing, Visualizing, and Analyzing Mass Spectrometry-Based Molecular Profile Data. *BMC Bioinformatics* **2010**, *11* (1), 395. https://doi.org/10.1186/1471-2105-11-395.
- (50) Katajamaa, M.; Miettinen, J.; Oresic, M. MZmine: Toolbox for Processing and Visualization of Mass Spectrometry Based Molecular Profile Data. *Bioinformatics* **2006**, 22 (5), 634–636. https://doi.org/10.1093/bioinformatics/btk039.
- (51) Roach, P. J.; Laskin, J.; Laskin, A. Higher-Order Mass Defect Analysis for Mass Spectra of Complex Organic Mixtures. *Anal. Chem.* **2011**, *83* (12), 4924–4929. https://doi.org/10.1021/ac200654j.
- (52) Choi, Y.; Vay, S. A.; Vadrevu, K. P.; Soja, A. J.; Woo, J.-H.; Nolf, S. R.; Sachse, G. W.; Diskin, G. S.; Blake, D. R.; Blake, N. J.; Singh, H. B.; Avery, M. A.; Fried, A.; Pfister, L.; Fuelberg, H. E. Characteristics of the Atmospheric CO2 Signal as Observed over the Conterminous United States during INTEX-NA. *Journal of Geophysical Research: Atmospheres* 2008, 113 (D7). https://doi.org/10.1029/2007JD008899.
- (53) Warner, J. X.; Wei, Z.; Strow, L. L.; Barnet, C. D.; Sparling, L. C.; Diskin, G.; Sachse, G. Improved Agreement of AIRS Tropospheric Carbon Monoxide Products with Other EOS Sensors Using Optimal Estimation Retrievals. *Atmospheric Chemistry and Physics* 2010, 10 (19), 9521–9533. https://doi.org/10.5194/acp-10-9521-2010.
- (54) Sachse, G. W.; Hill, G. F.; Wade, L. O.; Perry, M. G. Fast-Response, High-Precision Carbon Monoxide Sensor Using a Tunable Diode Laser Absorption Technique. *Journal of Geophysical Research: Atmospheres* **1987**, *92* (D2), 2071–2081. https://doi.org/10.1029/JD092iD02p02071.
- (55) FIREX-AQ Science Team. Fire Influence on Regional to Global Environments and Air Quality, 2019.

- https://doi.org/10.5067/SUBORBITAL/FI REXAO2019/DATA001.
- (56) Forster, C.; Wandinger, U.; Wotawa, G.; James, P.; Mattis, I.; Althausen, D.; Simmonds, P.; O'Doherty, S.; Jennings, S. G.; Kleefeld, C.; Schneider, J.; Trickl, T.; Kreipl, S.; Jäger, H.; Stohl, A. Transport of Boreal Forest Fire Emissions from Canada to Europe. *Journal of Geophysical Research: Atmospheres* **2001**, *106* (D19), 22887–22906.
 - https://doi.org/10.1029/2001JD900115.
- (57) DeBell, L. J.; Vozzella, M.; Talbot, R. W.; Dibb, J. E. Asian Dust Storm Events of Spring 2001 and Associated Pollutants Observed in New England by the Atmospheric Investigation, Regional Modeling, Analysis and Prediction (AIRMAP) Monitoring Network. *Journal of Geophysical Research:* Atmospheres 2004, 109 (D1). https://doi.org/10.1029/2003JD003733.
- (58) Tanimoto, H.; Matsumoto, K.; Uematsu, M. Ozone-CO Correlations in Siberian Wildfire Plumes Observed at Rishiri Island. *SOLA* **2008**, *4*, 65–68. https://doi.org/10.2151/sola.2008-017.
- (59) Liu, J.; Drummond, J. R.; Li, Q.; Gille, J. C.; Ziskin, D. C. Satellite Mapping of CO Emission from Forest Fires in Northwest America Using MOPITT Measurements. *Remote Sensing of Environment* **2005**, *95* (4), 502–516. https://doi.org/10.1016/j.rse.2005.01.009.
- (60) Ulbrich, I. M.; Canagaratna, M. R.; Zhang, Q.; Worsnop, D. R.; Jimenez, J. L. Interpretation of Organic Components from Positive Matrix Factorization of Aerosol Mass Spectrometric Data. *Atmospheric Chemistry and Physics* **2009**, *9* (9), 2891–2918. https://doi.org/10.5194/acp-9-2891-2009.
- (61) Chen, Y.; Xu, L.; Humphry, T.; Hettiyadura, A. P. S.; Ovadnevaite, J.; Huang, S.; Poulain, L.; Schroder, J. C.; Campuzano-Jost, P.; Jimenez, J. L.; Herrmann, H.; O'Dowd, C.; Stone, E. A.; Ng, N. L. Response of the Aerodyne Aerosol Mass Spectrometer to Inorganic Sulfates and Organosulfur Compounds: Applications in Field and Laboratory Measurements.

- Environ. Sci. Technol. **2019**, *53* (9), 5176–5186.
- https://doi.org/10.1021/acs.est.9b00884.
- (62) Guo, H.; Xu, L.; Bougiatioti, A.; Cerully, K. M.; Capps, S. L.; Hite, J. R.; Carlton, A. G.; Lee, S.-H.; Bergin, M. H.; Ng, N. L.; Nenes, A.; Weber, R. J. Fine-Particle Water and pH in the Southeastern United States. *Atmos. Chem. Phys.* 2015, 15 (9), 5211–5228. https://doi.org/10.5194/acp-15-5211-2015.
- (63) Budisulistiorini, S. H.; Riva, M.; Williams, M.; Chen, J.; Itoh, M.; Surratt, J. D.; Kuwata, M. Light-Absorbing Brown Carbon Aerosol Constituents from Combustion of Indonesian Peat and Biomass. *Environ. Sci. Technol.* 2017, 51 (8), 4415–4423. https://doi.org/10.1021/acs.est.7b00397.
- Fleming, L. T.; Lin, P.; Laskin, A.; Laskin, J.; Weltman, R.; Edwards, R. D.; Arora, N. K.; Yadav, A.; Meinardi, S.; Blake, D. R.; Pillarisetti, A.; Smith, K. R.; Nizkorodov, S. A. Molecular Composition of Particulate Matter Emissions from Dung and Brushwood Burning Household Cookstoves in Haryana, India. *Atmospheric Chemistry and Physics* 2018, 18 (4), 2461–2480. https://doi.org/10.5194/acp-18-2461-2018.
- (65) Simoneit, B. R. T.; Rogge, W. F.; Mazurek, M. A.; Standley, L. J.; Hildemann, L. M.; Cass, G. R. Lignin Pyrolysis Products, Lignans, and Resin Acids as Specific Tracers of Plant Classes in Emissions from Biomass Combustion. *Environ. Sci. Technol.* 1993, 27 (12), 2533–2541. https://doi.org/10.1021/es00048a034.
- (66) Lin, P.; Bluvshtein, N.; Rudich, Y.; Nizkorodov, S. A.; Laskin, J.; Laskin, A. Molecular Chemistry of Atmospheric Brown Carbon Inferred from a Nationwide Biomass Burning Event. *Environ. Sci. Technol.*2017, 51 (20), 11561–11570. https://doi.org/10.1021/acs.est.7b02276.
- (67) Iinuma, Y.; Böge, O.; Gräfe, R.; Herrmann, H. Methyl-Nitrocatechols: Atmospheric Tracer Compounds for Biomass Burning Secondary Organic Aerosols. *Environ. Sci. Technol.* 2010, 44 (22), 8453–8459. https://doi.org/10.1021/es102938a.
- (68) Borthakur, A.; Rao, V. S. B. Mass Spectral Studies of Alkylbenzenesulphonic Acids

- through Their S-Benzylisothiouronium Salts. *Organic Mass Spectrometry* **1984**, *19* (1), 48–53. https://doi.org/10.1002/oms.1210190109.
- (69) McCormack, P.; Jones, P.; Hetheridge, M. J.; Rowland, S. J. Analysis of Oilfield Produced Waters and Production Chemicals by Electrospray Ionisation Multi-Stage Mass Spectrometry (ESI-MSn). Water Research 2001, 35 (15), 3567–3578. https://doi.org/10.1016/S0043-1354(01)00070-7.
- (70) González-Mazo, E.; Honing, M.; Barceló, D.; Gómez-Parra, A. Monitoring Long-Chain Intermediate Products from the Degradation of Linear Alkylbenzene Sulfonates in the Marine Environment by Solid-Phase Extraction Followed by Liquid Chromatography/Ionspray Mass Spectrometry. *Environ. Sci. Technol.* **1997**, *31* (2), 504–510. https://doi.org/10.1021/es960333p.
- (71) Riu, J.; Gonzalez-Mazo, E.; Gomez-Parra, A.; Barceló, D. Determination of Parts per Trillion Level of Carboxylic Degradation Products of Linear Alkylbenzenesulfonates in Coastal Water by Solid-Phase Extraction Followed by Liquid Chromatography/Ionspray/Mass Spectrometry Using Negative Ion Detection. Chromatographia 1999, 50 (5-6),275–281. https://doi.org/10.1007/BF02490828.
- (72) Lyon, P. A.; Stebbings, W. L.; Crow, F. W.; Tomer, K. B.; Lippstreu, D. L.; Gross, M. L. Analysis of Anionic Surfactants by Mass Spectrometry/Mass Spectrometry with Fast Atom Bombardment. *Anal. Chem.* **1984**, *56* (1), 8–13. https://doi.org/10.1021/ac00265a004.
- (73) Zhao, H.; Xiang, L.; Li, J.; Yang, Z.; Fang, J.; Zhao, C.; Xu, S.; Cai, Z. Investigation on Fragmentation Pathways of Bisphenols by Using Electrospray Ionization Orbitrap Mass Spectrometry. *Rapid Communications in Mass Spectrometry* **2016**, *30* (16), 1901–1913. https://doi.org/10.1002/rcm.7666.
- (74) Cai, D.; Wang, X.; George, C.; Cheng, T.; Herrmann, H.; Li, X.; Chen, J. Formation of Secondary Nitroaromatic Compounds in Polluted Urban Environments. *Journal of*

- Geophysical Research: Atmospheres **2022**, 127 (10), e2021JD036167. https://doi.org/10.1029/2021JD036167.
- (75) Li, A.; Shi, X.; Qiu, X.; Wei, G.; Zheng, Y.; Chen, Q.; Chen, S.; Hu, M.; Zhu, T. Organosulfur Compounds in Ambient Fine Particulate Matter in an Urban Region: Findings of a Nontargeted Approach. *Science of The Total Environment* **2023**, 887, 164114. https://doi.org/10.1016/j.scitotenv.2023.164114.
- (76) Glasius, M.; Thomsen, D.; Wang, K.; Iversen, L. S.; Duan, J.; Huang, R.-J. Chemical Characteristics and Sources of Organosulfates, Organosulfonates, and Carboxylic Acids in Aerosols in Urban Xi'an, Northwest China. Science of The Total Environment 2022, 810, 151187. https://doi.org/10.1016/j.scitotenv.2021.151187.
- (77) Nguyen, T. B.; Lee, P. B.; Updyke, K. M.; Bones, D. L.; Laskin, J.; Laskin, A.; Nizkorodov, S. A. Formation of Nitrogen- and Sulfur-Containing Light-Absorbing Compounds Accelerated by Evaporation of Water from Secondary Organic Aerosols. *Journal of Geophysical Research: Atmospheres* **2012**, 117 (D1). https://doi.org/10.1029/2011JD016944.
- (78) Lobodin, V. V.; Marshall, A. G.; Hsu, C. S. Compositional Space Boundaries for Organic Compounds. *Anal. Chem.* **2012**, *84* (7), 3410–3416. https://doi.org/10.1021/ac300244f.
- (79) Cain, J.; Laskin, A.; Kholghy, M. R.; Thomson, M. J.; Wang, H. Molecular Characterization of Organic Content of Soot along the Centerline of a Coflow Diffusion Flame. *Phys. Chem. Chem. Phys.* **2014**, *16* (47), 25862–25875. https://doi.org/10.1039/C4CP03330B.

- (80) Qiu, L.; Psimos, M. D.; Cooks, R. G. Spontaneous Oxidation of Aromatic Sulfones to Sulfonic Acids in Microdroplets. *J. Am. Soc. Mass Spectrom.* **2022**, *33* (8), 1362–1367. https://doi.org/10.1021/jasms.2c00029.
- (81)Tsigaridis, K.; Daskalakis, N.; Kanakidou, M.; Adams, P. J.; Artaxo, P.; Bahadur, R.; Balkanski, Y.; Bauer, S. E.; Bellouin, N.; Benedetti, A.; Bergman, T.; Berntsen, T. K.; Beukes, J. P.; Bian, H.; Carslaw, K. S.; Chin, M.; Curci, G.; Diehl, T.; Easter, R. C.; Ghan, S. J.; Gong, S. L.; Hodzic, A.; Hoyle, C. R.; Iversen, T.; Jathar, S.; Jimenez, J. L.; Kaiser, J. W.; Kirkevåg, A.; Koch, D.; Kokkola, H.; Lee, Y. H.; Lin, G.; Liu, X.; Luo, G.; Ma, X.; Mann, G. W.; Mihalopoulos, N.; Morcrette, J.-J.; Müller, J.-F.; Myhre, G.; Myriokefalitakis, S.; Ng, N. L.; O'Donnell, D.; Penner, J. E.; Pozzoli, L.; Pringle, K. J.; Russell, L. M.; Schulz, M.; Sciare, J.; Seland, Ø.; Shindell, D. T.; Sillman, S.; Skeie, R. B.; Spracklen, D.; Stavrakou, T.; Steenrod, S. D.; Takemura, T.; Tiitta, P.; Tilmes, S.; Tost, H.; van Noije, T.; van Zyl, P. G.; von Salzen, K.; Yu, F.; Wang, Z.; Wang, Z.; Zaveri, R. A.; Zhang, H.; Zhang, K.; Zhang, Q.; Zhang, X. The AeroCom Evaluation and Intercomparison of Organic Aerosol in Global Models. Atmos. Chem. **2014**, *14* Phys. (19),10845-10895. https://doi.org/10.5194/acp-14-10845-2014.
- (82) Hodzic, A.; Kasibhatla, P. S.; Jo, D. S.; Cappa, C. D.; Jimenez, J. L.; Madronich, S.; Park, R. J. Rethinking the Global Secondary Organic Aerosol (SOA) Budget: Stronger Production, Faster Removal, Shorter Lifetime. *Atmos. Chem. Phys.* **2016**, *16* (12), 7917–7941. https://doi.org/10.5194/acp-16-7917-2016.